

(\*\*COMP: Special characters: **xxa** = alpha; **xxb** = beta; **xx'** = prime symbol; **xxm** = mu;  
**xxD** = u/c delta)

## SAHA SUPPRESSES PERITONEAL FIBROSIS IN MICE

5 Kumiko Io,<sup>1</sup> Tomoya Nishino,<sup>1</sup> Yoko Obata,<sup>1</sup> Mineaki Kitamura,<sup>1</sup> Takehiko Koji,<sup>2</sup> and  
Shigeru Kohno<sup>1</sup>

Second Department of Internal Medicine,<sup>1</sup> Nagasaki University School of Medicine,  
Nagasaki, Japan; and Department of Histology and Cell Biology,<sup>2</sup> Nagasaki University  
Graduate School of Biomedical Sciences, Nagasaki, Japan

10 HDACI FOR PERITONEAL FIBROSIS

IO *et al.*

Correspondence to: Tomoya Nishino, Second Department of Internal Medicine, Nagasaki

15 University School of Medicine, 1-7-1 Sakamoto, Nagasaki 852-8102, Japan.

[tnishino@nagasaki-u.ac.jp](mailto:tnishino@nagasaki-u.ac.jp)

[ABSTRACT]

*Objective:* Long-term peritoneal dialysis causes peritoneal fibrosis in submesothelial areas.

20 However, the mechanism of peritoneal fibrosis is unclear. Epigenetics is the mechanism to

induce heritable changes without any changes in DNA sequences. Among epigenetic modifications, histone acetylation leads to the transcriptional activation of genes. Recent studies indicate that histone acetylation is involved in the progression of fibrosis. Therefore, we examined the effect of suberoylanilide hydroxamic acid (SAHA), a histone deacetylase inhibitor, on the progression of peritoneal fibrosis in mice.

*Methods:* Peritoneal fibrosis was induced by the injection of chlorhexidine gluconate (CG) into the peritoneal cavity of mice every other day for 3 weeks. SAHA, or a dimethylsulfoxide and saline vehicle, was administered subcutaneously every day from the start of the CG injections for 3 weeks. Morphologic peritoneal changes were assessed by Masson's trichrome staining, and fibrosis-associated factors were assessed by immunohistochemistry.

*Results:* In CG-injected mice, a marked thickening of the submesothelial compact zone was observed. In contrast, the administration of SAHA suppressed the progression of submesothelial thickening and type III collagen accumulation in CG-injected mice. The numbers of fibroblast-specific protein-1–positive cells and  $\alpha$ -smooth muscle actin–positive cells were significantly decreased in the CG + SAHA group compared to that of the CG group. The level of histone acetylation was reduced in the peritoneum of the CG group, whereas it was increased in the CG + SAHA group.

*Conclusions:* Our results indicate that SAHA can suppress peritoneal thickening and fibrosis in mice through up-regulation of histone acetylation. These results suggest that SAHA may have therapeutic potential for treating peritoneal fibrosis.

**KEY WORDS:** Suberoylanilide hydroxamic acid, SAHA, histone deacetylase inhibitor, peritoneal fibrosis, chlorhexidine gluconate.

Although peritoneal dialysis (PD) is a beneficial treatment for patients with end-stage renal  
45 diseases, long-term PD causes morphologic and functional changes in the peritoneum (1).  
Characteristic pathologic findings in the peritoneum, related to long-term PD, include marked  
peritoneal fibrosis and massive accumulation of collagen in submesothelial areas (2, 3). In  
particular, some patients with peritoneal fibrosis develop encapsulating peritoneal sclerosis  
(EPS) associated with high mortality, which is one of the most critical complications in PD.  
50 However, the mechanism underlying peritoneal fibrosis in PD patients remains poorly  
understood and no effective therapy is available at present. To investigate the mechanism of  
peritoneal fibrosis and effective therapy, animal models of peritoneal fibrosis are used.  
Among them, chlorhexidine gluconate (CG) is often used to induce peritoneal fibrosis (4).  
This is a reversible model (5), therefore, repeat injections of CG need to be continued during  
55 the course of the experiment to induce persistent chemical irritation and tissue damage (6). In  
fact, following injection of CG, many pathologic findings in the peritoneum of PD patients,  
including increased expression of collagen III,  $\alpha$ -smooth muscle actin ( $\alpha$ SMA),  
macrophage infiltration, were also observed in previous studies (4,7). These similarities in  
alterations of the peritoneal membranes between experimental CG models and human PD  
60 patients strongly suggest that the CG model is a reasonable candidate model to examine the  
efficacy of various potential therapeutic reagents for regulating peritoneal sclerosis.

Epigenetics is defined as the mechanism to induce heritable change in the pattern of gene  
expression without any changes in DNA sequences (8). Epigenetic regulations depend on  
DNA methylation, histone modification, RNA interference, and so on. It has been shown that  
65 epigenetic modifications are involved in various human diseases, for example, cancer,  
hypertension, diabetes, and atherosclerosis (8). Moreover, a recent study has revealed that  
hypermethylation of rat sarcoma (RAS) protein activator like-1 (RASAL1) is associated with

the perpetuation of fibroblast activation and fibrogenesis in the kidney, leading to glomerular and interstitial fibrosis (9).

70 Among epigenetic regulation, global histone acetylation alters chromatin structure and regulates the dynamics of gene expression. The level of acetylation reflects a balance between histone acetyltransferase (HAT) and histone deacetylase (HDAC) protein families (10). Recently, it was demonstrated that HDACs are related to the progression of tissue fibrosis in multiple organs including kidney, heart and lung (11). A report showed that  
75 HDAC levels were increased and histone acetylation was decreased in kidneys injured by unilateral ureteral obstruction (UUO), which is a model of fibrosis (12). In addition, it has been reported that HDAC inhibitors (HDACi) are potentially therapeutic for fibrotic disorders because they have anti-fibrotic activity. Among HDACi, suberoylanilide hydroxamic acid (SAHA) has nonspecific HDAC-inhibition activity, affecting all classes of  
80 HDACs, and has received approval from the US Food and Drug Administration for treatment of refractory cutaneous T-cell lymphoma (13). SAHA exhibits relatively low toxicity towards normal cells compared to other HDACi (13). It was reported that SAHA attenuated mesangial collagen IV deposition in a mouse model of diabetic nephropathy (14). In addition, SAHA also attenuated collagen deposition in the ventricle and cell infiltration throughout the  
85 interstitium; thereby, improving cardiovascular remodeling in deoxycorticosterone acetate-salt hypertensive rats (15). Furthermore, previous reports indicate that inflammation plays an important role in the progression of organ fibrosis, and angiogenesis is associated with the development of fibrosis (16,17). It has been also reported that SAHA suppressed inflammation and angiogenesis (18,19). Therefore, we used SAHA as an HDACi in our  
90 present study.

Generally, increased levels of histone acetylation are associated with transcriptional activation (20). Some reports indicate that the expression of fibrosis inhibitory factors can be increased by promoting histone acetylation (21,22). As the effects of inhibitory factors for fibrosis, Yu *et al.* reported that bone morphogenetic protein 7 (BMP-7) and hepatocyte growth factor (HGF) ameliorated high-glucose–induced epithelial-to-mesenchymal transition (EMT) of peritoneal mesothelial cells (23). Inhibitors of DNA binding/differentiation 2 (Id2), which plays a role in inhibiting TGF- $\alpha$ –induced EMT in human renal epithelial cells, were shown to be upregulated, together with BMP-7, by HDACi (21).

In the present study, we hypothesized that HDACi could inhibit peritoneal fibrosis by promoting histone acetylation, following the increase of a fibrosis inhibitory factor; we focused on BMP-7. In this study, we investigated first the changes in histone acetylation in the CG-induced fibrotic peritoneum of mice. Then, we determined the effects of HDACi on fibrotic changes induced by CG.

Our results raise the possibility that HDACi may be a useful therapeutic agent for attenuating the progression of peritoneal fibrosis.

## METHODS

### ANIMAL MODELS

The experiments described in this study were conducted on 10-week-old male ICR mice  
110 (Japan SLC Inc., Shizuoka, Japan). They were housed in standard rodent cages in a light- and  
temperature-controlled room in the Biomedical Research Center, Center for Frontier Life  
Sciences, Nagasaki University. They had free access to laboratory food and tap water. The  
experimental protocol was inspected by the Animal Care and Use Committee of Nagasaki  
University, and approved by the President of Nagasaki University (Approval number:  
115 1004050846).

### EXPERIMENTAL PROTOCOL

Peritoneal fibrosis was induced by intraperitoneal injection of 0.1% CG in 15% ethanol  
dissolved in saline, as described previously, but with a slight modification (16,24). Mice  
received injections of 0.1% CG in 15% ethanol dissolved in saline (CG) or 15% ethanol  
120 dissolved in saline only at a dose of 0.3 mL/body into the peritoneal cavity every other day  
for 3 weeks. SAHA (10009929; Cayman Chemicals, MI, USA), which was dissolved in a  
vehicle (dimethylsulfoxide:saline = 1:1), or a vehicle alone, was administered subcutaneously,  
as previously reported (25). SAHA was administered at a dose of 25 mg/kg body weight  
every day for 3 weeks. Mice were assigned to 4 groups: (1) mice injected 15% ethanol  
125 dissolved in saline intraperitoneally and vehicle subcutaneously ( $n = 5$ ), defined as the  
control group; (2) mice injected 15% ethanol dissolved in saline intraperitoneally and SAHA  
subcutaneously ( $n = 5$ ), defined as SAHA group; (3) mice injected CG intraperitoneally and  
vehicle subcutaneously ( $n = 10$ ), defined as CG group; and (4) mice injected CG  
intraperitoneally and SAHA subcutaneously, defined as CG + SAHA group ( $n = 10$ ). The

130 dose and interval for administration of SAHA were selected on the basis of pilot studies  
conducted to determine the effects of different doses on the thickness of the submesothelial  
area. SAHA at a dose of 12.5 mg/kg body weight did not reduce peritoneal thickness  
compared with that in non-treated CG mice. SAHA at doses of 25 or 50 mg/kg body weight  
reduced peritoneal thickness to the same degree. Therefore, we selected 25 mg/kg body  
135 weight in the present study. No mice were excluded from the study once they were treated.

Mice were sacrificed at day 21 after the first CG injection, and peritoneal tissues were  
dissected out carefully. To avoid direct damage to the peritoneum due to repeated injections,  
CG was injected at the lower part of the peritoneum, whereas the upper portion of the parietal  
peritoneum was used for the examination. The tissues were fixed with 4% paraformaldehyde  
140 in phosphate-buffered saline (PBS; pH 7.4) immediately after sampling, and were embedded  
in paraffin. For morphological examination of the peritoneum, 4-xxmm thick, paraffin-  
embedded tissues were stained with Masson's trichrome staining.

## IMMUNOHISTOCHEMISTRY

Paraffin-embedded tissue sections were stained immunohistochemically using an indirect  
145 method (26). The following antibodies were used for immunohistochemistry: (1) rabbit anti-  
type III collagen antibody diluted 1:400 (LB-1393; LSL Co., Tokyo, Japan); (2) rabbit anti-  
human phosphorylated-Smad2/3 antibody diluted 1:50 (sc-11769-R; Santa Cruz  
Biotechnology, Santa Cruz, CA, USA); (3) rabbit anti-human fibroblast-specific protein-1  
(FSP-1) antibody diluted 1:100 (A5114; DAKO, Glostrup, Denmark); (4) mouse anti-human  
150 xxaSMA antibody diluted 1:50 (A2547; Sigma-Aldrich, St.Louis, US); (5) rat anti-mouse  
F4/80 antibody diluted 1:50 (MCA 497; Serotec, Kidlington, UK); and (6) goat anti-mouse  
PECAM/CD31 antibody diluted 1:50 (sc-1506; Santa Cruz Biotechnology).

After deparaffinization, the sections were treated with 0.3% H<sub>2</sub>O<sub>2</sub> for 20 min to inactivate endogenous peroxidase activity. For the immunohistochemical analysis of phosphorylated-Smad2/3 and CD31, the sections were treated in a microwave oven (MI-77; Azumaya, Tokyo, Japan) at 95°C for 5 or 15 min in 10 mmol/L citrate buffer (pH 6.0), before H<sub>2</sub>O<sub>2</sub> treatment for antigen retrieval. For the immunohistochemical analysis of type III collagen, FSP-1, F4/80 and xxaSMA, the sections were treated with proteinase K (P2308; Sigma, St Louis, MO) for 15 min at 37°C, before H<sub>2</sub>O<sub>2</sub> treatment for antigen retrieval. The sections were incubated for 30 min with a blocking solution (5% normal goat serum, 5% fetal calf serum, 5% bovine serum albumin (BSA), and 20% normal swine serum in PBS) at room temperature. The sections were then exposed to the primary antibody, which was diluted in the blocking buffer. For phosphorylated-Smad2/3 and CD31 staining, the sections were stained with the avidin–biotin complex by using a Vectastain Elite ABC kit (Vector Laboratories, Burlingame, CA, USA) after reacting with the primary antibody overnight at 4°C. For xxaSMA, the sections were exposed to a complex of anti-xxaSMA antibody and horseradish peroxidase (HRP)-conjugated rabbit anti-mouse immunoglobulin antibody (P0161; Dako) diluted 1:50 for 30 min at room temperature. Then, sections were incubated with the Envision<sup>+</sup> System-HRP Labelled Polymer Anti-Rabbit (K4002, Dako) for 30 min at room temperature. For type III collagen, FSP-1 and F4/80, after reacting with the primary antibodies for 1 h or overnight at room temperature, the sections were incubated with HRP-conjugated swine anti-rabbit immunoglobulin antibody (P0399; Dako) or rabbit anti-rat immunoglobulin antibody (P0450; Dako), diluted 1:50, for 30 min at room temperature. The reaction sites were visualized by treating the sections with H<sub>2</sub>O<sub>2</sub> and 3,3xx'-diaminobenzidine tetrahydrochloride (26). Finally, the sections were counterstained with methyl green and mounted. For all specimens, negative controls were prepared using normal IgG instead of the primary antibody.

## IMMUNOFLUORESCENCE STAINING

The following antibodies were used for immunofluorescence staining: (1) rabbit anti-human acetyl-histone H3 (Lys9) antibody, diluted 1:100 (#9671; Cell Signaling Technology, Danvers, MA, USA), and (2) goat anti-human BMP-7 antibody diluted 1:25 (SC-9305; Santa Cruz Biotechnology).

After deparaffinization, the sections were incubated for 30 min or 1 h with a blocking solution consisting of 500  $\mu$ g/mL normal goat IgG and 1% BSA in PBS at room temperature. The sections were then incubated with the primary antibodies, which were diluted in the same blocking solution. The sections were incubated with either Alexa Fluor dye (Molecular probes, Inc; Eugene, OR, USA) 594-labeled goat anti-rabbit IgG (A11012; Invitrogen, Paisley, UK) or Alexa Fluor dye 488-labeled rabbit anti-goat IgG (A11078; Invitrogen) for 1 h, stained with 4,6-diamidino-2-phenylindole (DAPI) for 1 min, and mounted. The sections were analyzed using a confocal laser scanning microscope (LSM 5 PASCAL; Carl Zeiss Co., Ltd., Obekochen, Germany), and the images were obtained. Normal rabbit or goat IgG was used as a negative control.

### MORPHOMETRIC ANALYSIS

To assess the extent of peritoneal thickening, we used digitized images and image analysis software (Lumina vision; MITANI Corporation, Tokyo, Japan). We measured the thickness of the submesothelial zone above the abdominal muscle in cross-sections of the abdominal wall. The diameter of the  $\times 200$  magnification is 1 mm. For each sample, 5 such areas were selected and type III collagen-positive areas were determined. In each peritoneal sample, the numbers of phosphorylated-Smad2/3-positive cells, cells expressing FSP-1,  $\alpha$ SMA, F4/80 or BMP-7, CD31-positive vessels and submesothelial cells were counted in 5 fields at  $\times 200$  magnification.

## QUANTITATIVE RT-PCR

Quantitative real-time RT-PCR was performed as previously described (27). RNA was isolated from the peritoneum with 600  $\mu$ L RNA lysis buffer using an RNeasy Mini Kit (QIAGEN, Tokyo, Japan). Complementary DNA was reverse-transcribed using a high-capacity reverse transcription kit (Applied Biosystems, Life Technologies Japan Ltd., Tokyo, Japan). Approximately 25 ng cDNA was used as a template in reactions with 0.5  $\mu$ M of forward and reverse primers and SYBR Green (Applied Biosystems). Reactions were carried out using the StepOne Plus Real-Time PCR system, and quantitative comparisons were obtained using the  $2^{-\Delta\Delta C_T}$  method (Applied Biosystem). The following primers were used in reactions: *actin*, 5'-CATCCGTAAAGACCTCTATGCCAC-3' (forward) and 5'-ATGGAGCCACCATCCACA-3' (reverse) (28); *BMP-7*, 5'-CACTCCCTCCTCAACCCTCGGCA-3' (forward) and 5'-TAGAGGCATCATAGGCCAGGTGCCC-3' (reverse) (29);  $\alpha 1$  chain of type I collagen (*COL1 $\alpha$ 1*), 5'-TGGTCCTGCCGGTCCTCCTG-3' (forward) and 5'-ACACATTGGGGGTAGGAACA-3' (reverse) (30); Fibronectin, 5'-GAAACGGCCAACTCCGTCAC-3' (forward) and 5'-TGGGGTGCCAGTGGTCTCTT-3' (reverse) (31); Connective tissue growth factor (*CTGF*), 5'-TGCCAGAACGCACACTGAGG-3' (forward) and 5'-ATTGCCCTCCCCGGTTACAC-3' (reverse) (31).

## STATISTICAL ANALYSIS

Data were expressed as mean  $\pm$  standard error mean (SEM). Differences among groups were examined for statistical significance by using repeated measures analysis of variance (Bonferroni/Dunn test). A *p* value of  $< 0.05$  denoted statistically significant difference.

## RESULTS

### SAHA PREVENTED THE PERITONEAL FIBROSIS

Morphological changes were assessed using Masson's trichrome staining (Figure 1). In the normal mice, the peritoneal tissue comprised a peritoneal mesothelial monolayer and an  
230 exiguity of connective tissues under the mesothelial layer (Figure 1A). In the control group, the peritoneal tissues were almost normal and without thickening of the submesothelial zone (Figure 1B). On the other hand, the peritoneal samples from the mice in the CG group had a marked thickening of the submesothelial compact zone and a heavy infiltration of various cells at day 21 (Figure 1C). However, subcutaneous injection of SAHA prevented the  
235 progression of submesothelial thickening and reduced the number of cells in the CG + SAHA group (Figure 1D). A significant difference between the CG group and the CG + SAHA group was seen in the area of the submesothelial compact zone ( $p < 0.05$ , Figure 1E). The thickening of the peritoneum was not affected following repeated injections of SAHA compared with that of the control group (data not shown).

240 For the analysis of collagen deposition, we conducted the immunohistochemistry for type III collagen at day 21. As shown in Figure 2, in the control group, type III collagen expression in the submesothelial compact zone was marginal and equivalent to that of normal mice (Figure 2A). In the CG group, type III collagen was diffusely expressed in the submesothelial compact zone, whereas this expression was clearly decreased in the CG + SAHA group  
245 (Figure 2B, 2C). When we examined the signal for type III collagen quantitatively, the expression of type III collagen was higher in the CG group than in the control group, but was significantly lower in the CG + SAHA group than in the CG group (Figure 2E).

The expression of FSP-1, which is a marker of fibroblasts, was examined by immunohistochemistry. A few FSP-1–positive cells were in the peritoneum of the control group (data not shown). In the CG group, the number of FSP-1–positive cells increased  
250 markedly compared to that in the control group, and the treatment of SAHA inhibited these expressions significantly (Figure 3A – 3D). Furthermore, we examined the expression of  $\alpha$ SMA, which is a marker of myofibroblasts, by immunohistochemistry. In the control group, a few  $\alpha$ SMA–positive cells were found in the peritoneum (data not shown). The CG  
255 group showed a significant increase of  $\alpha$ SMA–positive cells, and in the CG + SAHA group, the number of  $\alpha$ SMA–positive cells was markedly decreased (Figure 3E – 3H).

#### SAHA SUPPRESSED TRANSFORMING GROWTH FACTOR (TGF)- $\beta$ SIGNALING

We examined TGF- $\beta$  signaling by performing immunohistochemistry for phosphorylated-Smad2/3, which is known as a mediator of TGF- $\beta$  signaling in regulation of the fibrotic  
260 response (Figure 4). In the control group, very few phosphorylated-Smad2/3–positive cells were observed in the peritoneum (data not shown). Treatment with CG significantly increased the number of phosphorylated-Smad2/3–positive cells in the thickened submesothelial compact zone compared with that in the control group (Figure 4A).  
Compared with that in the CG group, the number of positive cells was markedly reduced in  
265 the CG + SAHA group (Figure 4B, 4D).

Next, we investigated the expression of TGF- $\beta$ -dependent pro-fibrotic genes in the peritoneum tissue using real-time RT-PCR (Figure 4E – 4G). In the CG group, *COL1 $\alpha$ 1*, fibronectin and *CTGF* mRNA levels were higher than the control group. On the other hand, *COL1 $\alpha$ 1*, fibronectin and *CTGF* mRNA levels showed a tendency to be lower in the SAHA  
270 group.

## SAHA INCREASED THE LEVEL OF HISTONE ACETYLATION

Using immunofluorescence technique, we examined the level of H3K9 acetylation, which is representative of histone acetylation, in the cells of the submesothelial compact zone (Figure 5). H3K9 acetylation was low in the cells of the peritoneum of the control group (Figure 5A).  
275 In the CG group, moderate H3K9 acetylation was observed in the thickened submesothelial compact zone. In contrast, in the CG + SAHA group, the level of H3K9 acetylation tended to be higher than that in the CG group (Figure 5B, 5C).

## SAHA INCREASED THE EXPRESSION OF BMP-7

280 Next, we focused on BMP-7 as an inhibitory factor for fibrosis that is upregulated by the administration of HDACi (21). As shown in Figure 6, we examined the ratio of BMP-7–positive cells to all submesothelial cells in the submesothelial compact zone. In the control group, a few BMP-7–positive cells were detected in the peritoneum (Figure 6A). Although in the CG group some BMP-7–positive cells were in the submesothelial compact zone, the ratio  
285 of BMP-7–positive cells was significantly increased in the CG + SAHA group compared with that in the CG group (Figure 6B – 6E). The *BMP-7* mRNA level in the CG + SAHA group was significantly higher than levels in the CG group (Figure 6F).

## SAHA SUPPRESSED INFLAMMATION AND ANGIOGENESIS

To examine anti-inflammatory and anti-angiogenic effects by SAHA in peritoneal tissues, we  
290 used immunohistochemistry for F4/80 and CD31, which are markers of macrophages or dendritic cells, and vessels respectively (Figure 7A – 7H). In the peritoneum of the CG + SAHA group, the numbers of both F4/80–positive cells and CD31–positive vessels were less than those of the CG group. We identified anti-inflammatory and anti-angiogenic effects of SAHA in models of peritoneal fibrosis.

295 **DISCUSSION**

Our results indicated that SAHA effectively ameliorated peritoneal fibrosis. In addition, we confirmed that SAHA, as an HDAC inhibitor, promoted histone acetylation in the submesothelial compact zone of the peritoneum. Our study supports the existing data and reveals the beneficial effects of HDACi on fibrotic diseases. Previous studies described the effects of HDACi in various animal models, including heart failure (9), unilateral ureteral obstruction (8), and diabetic nephropathy (32). However, to our knowledge, this is the first study to investigate whether HDACi have inhibitory effects on peritoneal fibrosis.

Because increased levels of histone acetylation are usually associated with transcriptional activation (20), we speculated that the promotion of histone acetylation could be an effective strategy for the suppression of peritoneal fibrosis. In the present study, we focused on the expression of BMP-7 among fibrosis inhibitory factors. It is an endogenous protein that belongs to the TGF- $\alpha$  superfamily and is known to prevent the development of fibrosis in various organs (33–35). BMP-7 has been suggested to suppress fibrosis by inhibiting TGF- $\alpha$  synthesis (36) and by controlling TGF- $\alpha$  signaling via blocking the nuclear translocation of phosphorylated Smad2/3 (37). In fact, the association between BMP-7 and histone acetylation has been already shown (22). Marumo, *et al.* reported that marked induction of BMP-7 and the increase of strongly positive cells for acetylated histone were observed simultaneously in the proximal tubular cells during the recovery phase following renal ischemic reperfusion in mice (22). We also confirmed that the number of BMP-7–positive cells increased in the submesothelial compact zone in the CG + SAHA group compared with that in the CG group, and our results suggested that BMP-7 is involved in the suppression of peritoneal fibrosis, where it inhibits TGF- $\alpha$  signaling. Although we do not yet understand the difference observed between the levels of *BMP-7* mRNA and protein level

in the control group, this difference could have been caused by post-transcriptional regulation  
320 of protein synthesis, including mRNA stability and translational efficiency (38).

In this study, the peritoneal samples from mice in the CG group had a marked thickening of  
the submesothelial compact zone and a heavy infiltration of various cells at day 21. The  
results of immunohistochemistry for F4/80, FSP-1 and  $\alpha$ SMA suggested that a heavy  
infiltration of various cells in the peritoneum were mainly macrophages or dendritic cells,  
325 and myofibroblasts. The SAHA group had fewer inflammatory cells and myofibroblasts, in  
addition to displaying an inhibition of angiogenesis. Therefore, SAHA might have  
ameliorated peritoneal fibrosis by not only increasing the expression of BMP-7 but also  
inhibiting inflammation or angiogenesis.

Our study has some limitations for clinical application. First, there are some differences  
330 between CG-induced peritoneal fibrosis and human peritoneal fibrosis. CG models induce a  
chemical irritant but the etiology of human EPS is more complicated (4). However, most of  
the histological changes in CG models are similar to peritoneal fibrosis in humans —  
injection of CG results in progression of fibrosis and thickening of the peritoneum similar to  
human peritoneal fibrosis. Second, we started the administration of SAHA and CG  
335 simultaneously; the effect of SAHA as a therapeutic intervention subsequent to starting CG is  
unknown. Therefore, we anticipate further investigation into the therapeutic effect of SAHA.  
Third, the dosage of SAHA used in our study was almost 3 times that used clinically in the  
treatment of human cutaneous T cell lymphoma. There were no side effects such as liver or  
kidney dysfunction and the increase in mortality between the CG + SAHA group and the  
340 control group in our investigation. The effective and safe dose of SAHA for mice may be  
different from that used for humans. Further studies are needed to clarify whether SAHA can

be used to reduce peritoneal fibrosis in PD patients and to examine the suitable dose of SAHA for humans.

345 In conclusion, we have shown for the first time that SAHA inhibits the progression of peritoneal fibrosis in a mouse CG-induced peritoneal fibrosis model. Our result might be consistent with our hypothesis that SAHA inhibits the expression of fibrosis-associated factors via induction of BMP-7. Thus, SAHA represents a novel potential candidate for the treatment of peritoneal fibrosis.

### **ACKNOWLEDGEMENTS**

350 This work was supported by JSPS KAKENHI Grant-in-Aid for Young Scientists (B) Number 23790947 and grants from the Japanese Association of Dialysis Physicians. We would like to thank Ms. Ryoko Yamamoto and Ms. Shiho Kondo for excellent experimental assistance.

### **DISCLOSURES**

All authors state that they have no conflicts of interest to declare.

**REFERENCES**

1. Afthentopoulos IE, Passadakis P, Oreopoulos DG, Bargman J. Sclerosing peritonitis in continuous ambulatory peritoneal dialysis patients: One center's experience and review of the literature. *Adv Ren Replace Ther* 1998; 5:157–67.  
360
2. Gandhi VC, Humayun HM, Ing TS, Daugirdas JT, Jablokow VR, Iwatsuki S, *et al.* Sclerotic thickening of the peritoneal membrane in maintenance peritoneal dialysis patients. *Arch Intern Med* 1980; 140:1201–3.
3. Williams JD, Craig KJ, Topley N, Von Ruhland C, Fallon M, Newman GR, *et al.* Morphologic changes in the peritoneal membrane of patients with renal disease. *J Am Soc Nephrol* 2002; 13:470–9.  
365
4. Park SH, Kim YL, Lindholm B. Experimental encapsulating peritoneal sclerosis models: Pathogenesis and treatment. *Perit Dial Int* 2008; 28 Suppl 5:S21–8.
5. Sekiguchi Y, Hamada C, Ro Y, Nakamoto H, Inaba M, Shimaoka T, *et al.* Differentiation of bone marrow-derived cells into regenerated mesothelial cells in peritoneal remodeling using a peritoneal fibrosis mouse model. *J Artif Organs* 2012 Sep;; 15:272–82.  
370
6. Arai H, Furusu A, Nishino T, Obata Y, Nakazawa Y, Nakazawa M, *et al.* Thalidomide prevents the progression of peritoneal fibrosis in mice. *Acta Histochem Cytochem* 2011; 44:51–60.

- 7375 Hirose M, Nishino T, Obata Y, Nakazawa M, Nakazawa Y, Furusu A, *et al.* 22-oxacalcitriol prevents progression of peritoneal fibrosis in a mouse model. *Perit Dial Int* 2013 Mar–Apr; 33:132–42.
8. Dwivedi RS, Herman JG, McCaffrey TA, Raj DS. Beyond genetics: Epigenetic code in chronic kidney disease. *Kidney Int* 2011; 79:23–32.
- 9380 Bechtel W, McGoohan S, Zeisberg EM, Muller GA, Kalbacher H, Salant DJ, *et al.* Methylation determines fibroblast activation and fibrogenesis in the kidney. *Nat Med* 2010; 16:544–50.
10. Wiech NL, Fisher JF, Helquist P, Wiest O. Inhibition of histone deacetylases: A pharmacological approach to the treatment of non-cancer disorders. *Curr Top Med Chem* 385 2009; 9:257–71.
11. Pang M, Zhuang S. Histone deacetylase: A potential therapeutic target for fibrotic disorders. *J Pharmacol Exp Ther* 2010; 335:266–72.
12. Marumo T, Hishikawa K, Yoshikawa M, Hirahashi J, Kawachi S, Fujita T. Histone deacetylase modulates the proinflammatory and -fibrotic changes in tubulointerstitial injury. 390 *Am J Physiol Renal Physiol* 2010; 298:F133–41.
13. Ververis K, Hiong A, Karagiannis TC, Licciardi PV. Histone deacetylase inhibitors (hdacis): Multitargeted anticancer agents. *Biologics* 2013; 7:47–60.
14. Advani A, Huang Q, Thai K, Advani SL, White KE, Kelly DJ, *et al.* Long-term administration of the histone deacetylase inhibitor vorinostat attenuates renal injury in 395 experimental diabetes through an endothelial nitric oxide synthase-dependent mechanism. *Am J Pathol* 2011 May; 178:2205–14.

15. Iyer A, Fenning A, Lim J, Le GT, Reid RC, Halili MA, *et al.* Antifibrotic activity of an inhibitor of histone deacetylases in doca-salt hypertensive rats. *Br J Pharmacol* 2010; 159:1408–17.
- 160 16. Yoshio Y, Miyazaki M, Abe K, Nishino T, Furusu A, Mizuta Y, *et al.* Tnp-470, an angiogenesis inhibitor, suppresses the progression of peritoneal fibrosis in mouse experimental model. *Kidney Int* 2004; 66:1677–85.
17. Mishima Y, Miyazaki M, Abe K, Ozono Y, Shiohita K, Xia Z, *et al.* Enhanced expression of heat shock protein 47 in rat model of peritoneal fibrosis. *Perit Dial Int* 2003; 23:14–22.
- 185 18. Leoni F, Zaliani A, Bertolini G, Porro G, Pagani P, Pozzi P, *et al.* The antitumor histone deacetylase inhibitor suberoylanilide hydroxamic acid exhibits antiinflammatory properties via suppression of cytokines. *Proc Natl Acad Sci U S A* 2002; 99:2995–3000.
19. Deroanne CF, Bonjean K, Servotte S, Devy L, Colige A, Clause N, *et al.* Histone deacetylases inhibitors as anti-angiogenic agents altering vascular endothelial growth factor  
410 signaling. *Oncogene* 2002; 21:427–36.
20. Struhl K. Histone acetylation and transcriptional regulatory mechanisms. *Genes Dev* 1998; 12:599–606.
21. Yoshikawa M, Hishikawa K, Marumo T, Fujita T. Inhibition of histone deacetylase activity suppresses epithelial-to-mesenchymal transition induced by tgf-beta1 in human renal  
415 epithelial cells. *J Am Soc Nephrol* 2007; 18:58–65.
22. Marumo T, Hishikawa K, Yoshikawa M, Fujita T. Epigenetic regulation of bmp7 in the regenerative response to ischemia. *J Am Soc Nephrol* 2008; 19:1311–20.

23. Yu MA, Shin KS, Kim JH, Kim YI, Chung SS, Park SH, *et al.* Hgf and bmp-7 ameliorate high glucose-induced epithelial-to-mesenchymal transition of peritoneal mesothelium. *J Am Soc Nephrol* 2009; 20:567–81.
24. Nishino T, Miyazaki M, Abe K, Furusu A, Mishima Y, Harada T, *et al.* Antisense oligonucleotides against collagen-binding stress protein hsp47 suppress peritoneal fibrosis in rats. *Kidney Int* 2003; 64:887–96.
25. Van Beneden K, Geers C, Pauwels M, Mannaerts I, Verbeelen D, van Grunsven LA, *et al.* Valproic acid attenuates proteinuria and kidney injury. *J Am Soc Nephrol* 2011; 22:1863–75.
26. Song N, Liu J, An S, Nishino T, Hishikawa Y, Koji T. Immunohistochemical analysis of histone h3 modifications in germ cells during mouse spermatogenesis. *Acta Histochem Cytochem* 2011; 44:183–90.
27. Davis KM, Nakamura S, Weiser JN. Nod2 sensing of lysozyme-digested peptidoglycan promotes macrophage recruitment and clearance of *S. Pneumoniae* colonization in mice. *J Clin Invest* 2011; 121:3666–76.
28. Oyamada N, Sone M, Miyashita K, Park K, Taura D, Inuzuka M, *et al.* The role of mineralocorticoid receptor expression in brain remodeling after cerebral ischemia. *Endocrinology* 2008; 149:3764–77.
29. De Petris L, Hruska KA, Chiechio S, Liapis H. Bone morphogenetic protein-7 delays podocyte injury due to high glucose. *Nephrol Dial Transplant* 2007; 22:3442–50.
30. Manson SR, Song JB, Hruska KA, Austin PF. The hdac-dependent transcriptional repression of bmp-7 potentiates tgf-beta-mediated renal fibrosis in obstructive uropathies. *J Urol* 2013 Jun 29. Epub ahead of print.

- 3440 Pagel CN, Song SJ, Loh LH, Tudor EM, Murray-Rust TA, Pike RN, *et al.* Thrombin-stimulated growth factor and cytokine expression in osteoblasts is mediated by protease-activated receptor-1 and prostanoids. *Bone* 2009; 44:813–21.
32. Noh H, Oh EY, Seo JY, Yu MR, Kim YO, Ha H, *et al.* Histone deacetylase-2 is a key regulator of diabetes- and transforming growth factor-beta1-induced renal injury. *Am J Physiol Renal Physiol* 2009; 297:F729–39.
- 445
33. Hruska KA, Guo G, Wozniak M, Martin D, Miller S, Liapis H, *et al.* Osteogenic protein-1 prevents renal fibrogenesis associated with ureteral obstruction. *Am J Physiol Renal Physiol* 2000; 279:F130–43.
34. Zeisberg EM, Tarnavski O, Zeisberg M, Dorfman AL, McMullen JR, Gustafsson E, *et al.* Endothelial-to-mesenchymal transition contributes to cardiac fibrosis. *Nat Med* 2007; 13:952–61.
- 450
35. Zeisberg M, Yang C, Martino M, Duncan MB, Rieder F, Tanjore H, *et al.* Fibroblasts derive from hepatocytes in liver fibrosis via epithelial to mesenchymal transition. *J Biol Chem* 2007; 282:23337–47.
- 365
- Zhang XL, Selbi W, de la Motte C, Hascall V, Phillips AO. Bone morphogenic protein-7 inhibits monocyte-stimulated tgf-beta1 generation in renal proximal tubular epithelial cells. *J Am Soc Nephrol* 2005; 16:79–89.
37. Boon MR, van der Horst G, van der Pluijm G, Tamsma JT, Smit JW, Rensen PC. Bone morphogenetic protein 7: A broad-spectrum growth factor with multiple target therapeutic
- 460
- potency. *Cytokine Growth Factor Rev* 2011; 22:221–9.

38. Schindler R, Clark BD, Dinarello CA. Dissociation between interleukin-1 beta mrna and protein synthesis in human peripheral blood mononuclear cells. *J Biol Chem* 1990; 265:10232–7.

**FIGURE LEGENDS**

470 Figure 1 — The result of Masson's trichrome staining of peritoneal tissues. (A) In normal mice, the monolayer of mesothelial cells covered the entire surface of the peritoneum. (B) In the control group, peritoneal tissues were almost normal without thickening of the submesothelial zone. (C) The peritoneal tissues of the mice in the CG group showed marked thickening of the submesothelial compact zone and presence of numerous cells. (D) SAHA significantly prevented the progression of submesothelial thickening. (A–D), magnification 200×; bars indicate the thickness of the submesothelial compact zone. (E) Bar graph showing the thickness of the submesothelial compact zone. Data are expressed as mean±SEM; \* represents  $p<0.05$ .

480 Figure 2 — The result of the immunohistochemical analysis for type III collagen. (A) In the control group, type III collagen expression in the submesothelial compact zone was equivalent to that of normal mice. (B) In the CG group, type III collagen was diffusely expressed in the submesothelial compact zone. (C) Type III collagen expression was clearly decreased in the CG+SAHA group. (D) The peritoneal tissue of CG+SAHA group was incubated with normal IgG instead of type III collagen antibody as a negative control. (A–D), magnification 200×; bars indicate the thickness of the submesothelial compact zone. (E) Bar graph showing the positive areas for type III collagen. Data are expressed as mean±SEM; \* represents  $p<0.05$ .

490 Figure 3 — The result of the immunohistochemical analysis for FSP-1 and  $\alpha$ SMA. (A) The number of FSP-1–positive cells increased markedly in the CG group. (B) The expression of

FSP-1 was inhibited in the CG+SAHA group. (C) The peritoneal tissue of CG+SAHA group was incubated with normal IgG instead of FSP-1 antibody as a negative control. (A-C), magnification 200×; bars indicate the thickness of the submesothelial compact zone. (D) Bar graph showing the number of FSP-1–positive cells. Data are expressed as mean ± SEM; \* represents  $p < 0.05$ . (E) In the CG group, the number of  $\alpha$ SMA–positive cells was increased. (F) The number of  $\alpha$ SMA–positive cells was reduced in the CG+SAHA group. (G) The peritoneal tissue of CG+SAHA group was incubated with normal IgG instead of  $\alpha$ SMA antibody as a negative control. (E–G), magnification 200×; bars indicate the thickness of the submesothelial compact zone. (H) Bar graph showing the number of  $\alpha$ SMA–positive cells. Data are expressed as mean ± SEM; \* represents  $p < 0.05$ .

Figure 4 — The results of immunohistochemical analysis for phosphorylated Smad2/3 and TGF- $\beta$  dependent profibrotic genes expression.

(A) In the CG group, a number of phosphorylated-Smad2/3 positive cells were observed in thickened peritoneal compact zone. (B) These numbers were significantly decreased in the CG+SAHA group. (C) The peritoneal tissue of CG+SAHA group was incubated with normal IgG instead of phosphorylated Smad2/3 antibody as a negative control. (A–C), magnification 200×; bars indicate the thickness of the submesothelial compact zone. (D) Bar graph showing the number of phosphorylated-Smad2/3–positive cells. Data are expressed as mean ± SEM; \* represents  $p < 0.05$ . (E) *COL1 $\alpha$ 1* expression levels were measured by quantitative RT-PCR relative to  $\beta$ -actin controls. Values are relative to the control group ± SEM; \* represents  $p < 0.05$ . (F) Fibronectin expression levels were measured by quantitative RT-PCR relative to  $\beta$ -actin controls. Values are relative to the control group ± SEM; \* represents  $p < 0.05$ . (G)

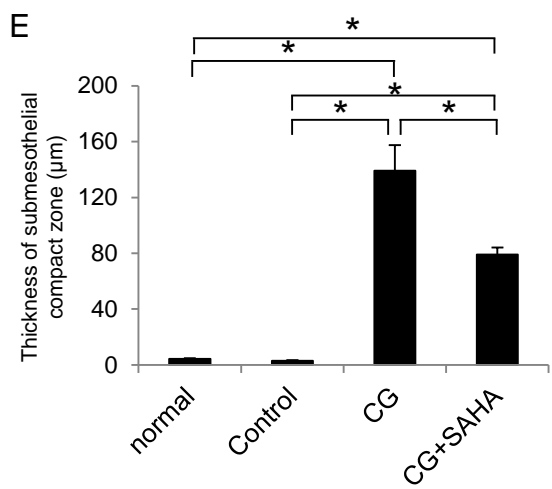
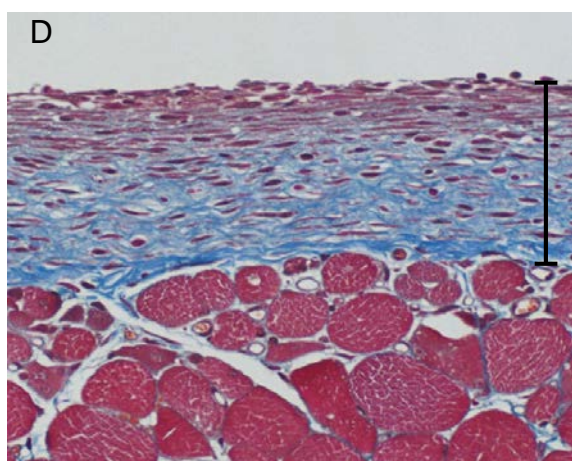
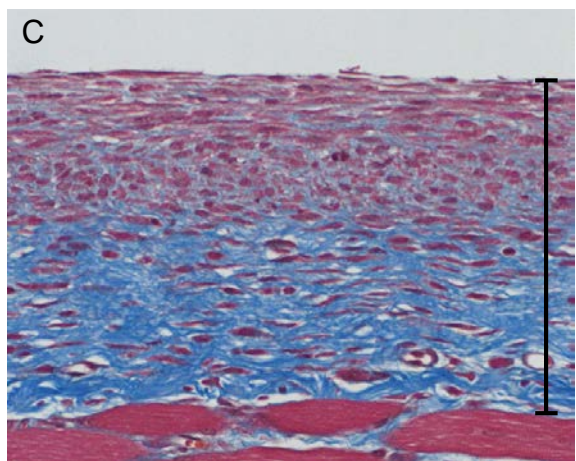
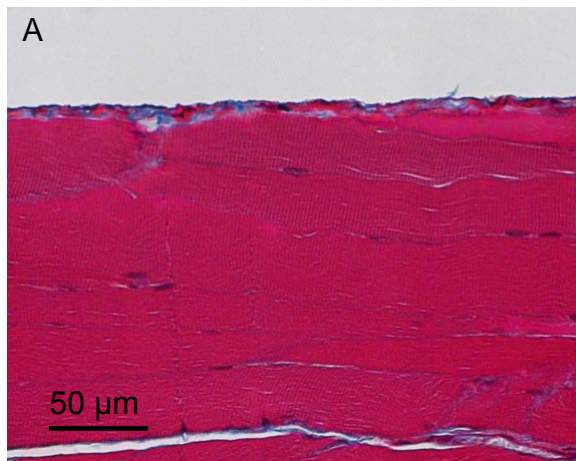
515 *CTGF* expression levels were measured by quantitative RT-PCR relative to *xxb-actin*  
controls. Values are relative to the control group $\pm$ SEM; \* represents  $p<0.05$ .

Figure 5 — The result of the immunofluorescence staining for H3K9 acetylation. (A) The  
control group showed low level of H3K9 acetylation in the cells of the peritoneum. (B) In the  
520 CG group, moderate level of H3K9 acetylation was evident by the thickened submesothelial  
compact zone. (C) In the CG+SAHA group, the level of H3K9 acetylation tended to be  
higher than that in the CG group. (D) The peritoneal tissue of CG+SAHA group was  
incubated with normal IgG instead of H3K9 acetylation antibody as a negative control. (A–  
D), magnification 200 $\times$ ; bars indicate the thickness of the submesothelial compact zone.

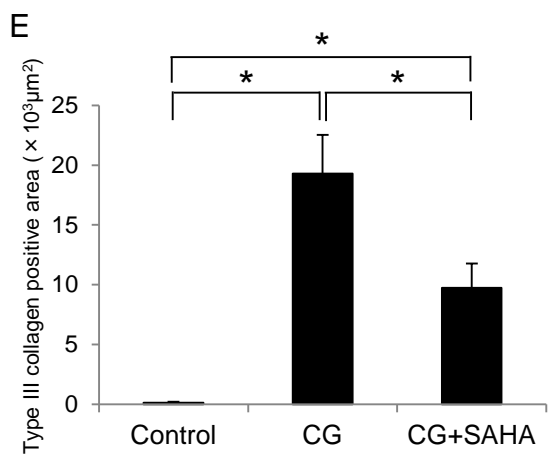
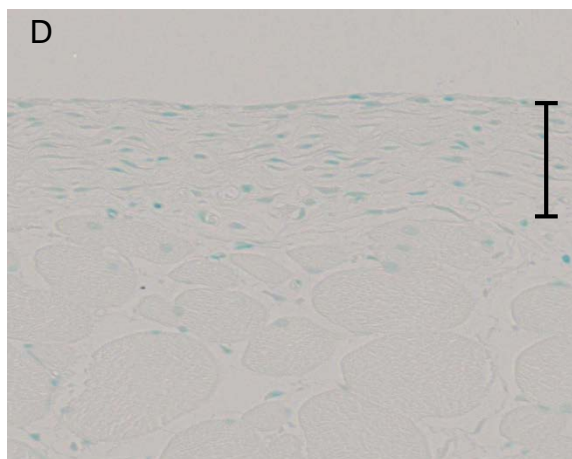
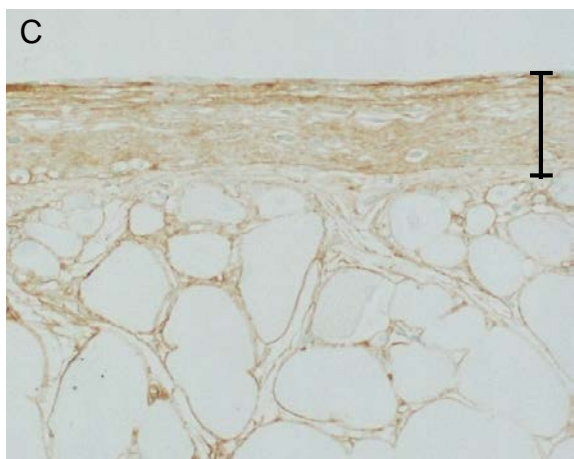
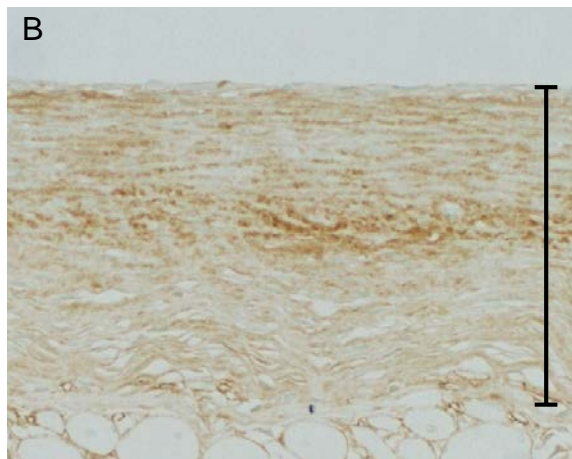
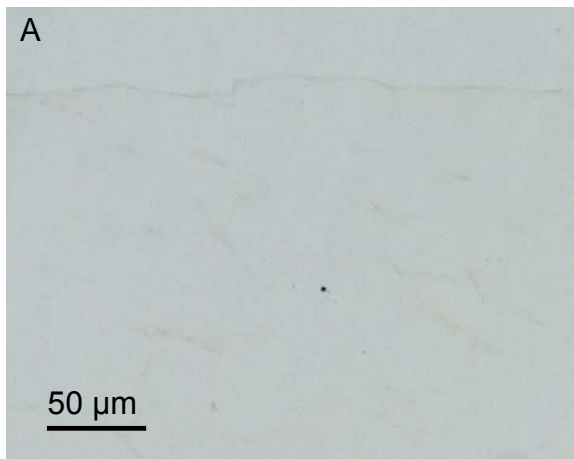
525

Figure 6 — The result of the immunofluorescence staining for BMP-7. (A) In the control  
group, very few BMP-7–positive cells were shown in the peritoneum. (B) The CG group  
showed some BMP-7–positive cells in the submesothelial compact zone. (C) The BMP-7–  
positive cells were increased in the CG+SAHA group. (D) The peritoneal tissue of  
530 CG+SAHA group was incubated with normal IgG instead of BMP-7 antibody as a negative  
control. (A–D), magnification 200 $\times$ ; bars indicate the thickness of the submesothelial  
compact zone. (E) Bar graph showing the BMP-7–positive cells. Data are expressed as  
mean $\pm$ SEM; \* represents  $p<0.05$ . (F) *BMP-7* expression levels were measured by  
quantitative real-time RT-PCR relative to *xxb-actin* controls. Values are relative to the  
535 control group $\pm$ SEM; \* represents  $p<0.05$ .

Figure 7 — The result of the immunohistochemical analysis for F4/80 and CD31. (A) In the CG group, a number of F4/80–positive cells were observed in thickened peritoneal compact zone. (B) These numbers were significantly decreased in the CG+SAHA group. (C) The peritoneal tissue of CG+SAHA group was incubated with normal IgG instead of F4/80 antibody as a negative control. (A–C), magnification 200×; bars indicate the thickness of the submesothelial compact zone. (D) Bar graph showing the number of F4/80–positive cells. Data are expressed as mean±SEM; \* represents  $p<0.05$ . (E) The number of CD31–positive vessels increased markedly in the CG group. (F) The number of CD31–positive vessels was reduced in the CG+SAHA group. (G) The peritoneal tissue of CG+SAHA group was incubated with normal IgG instead of CD31 antibody as a negative control. (E–G), magnification 200×; bars indicate the thickness of the submesothelial compact zone. (H) Bar graph showing the number of CD31–positive vessels. Data are expressed as mean±SEM; \* represents  $p<0.05$ .



**Fig 1**



**Fig 2**

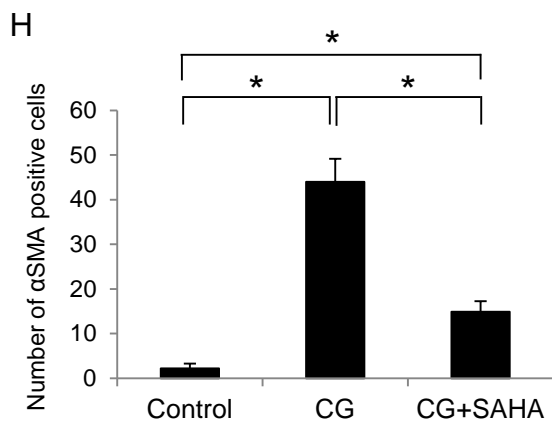
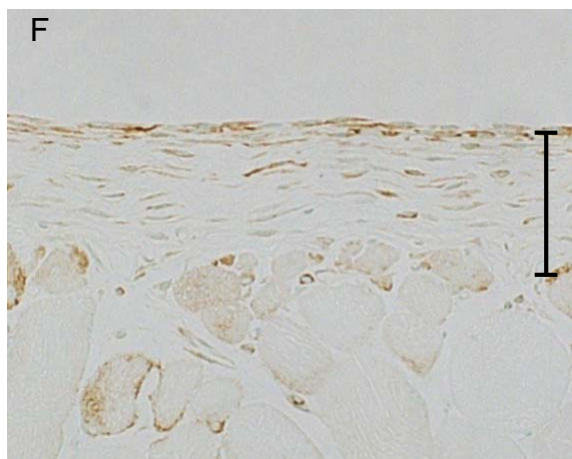
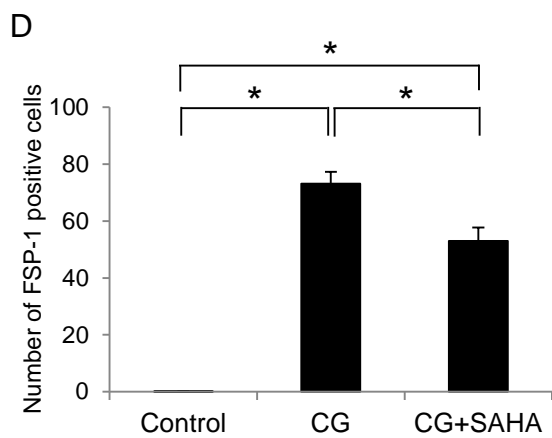
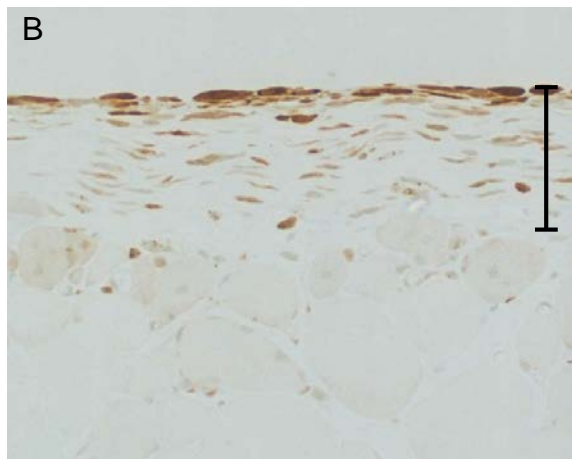
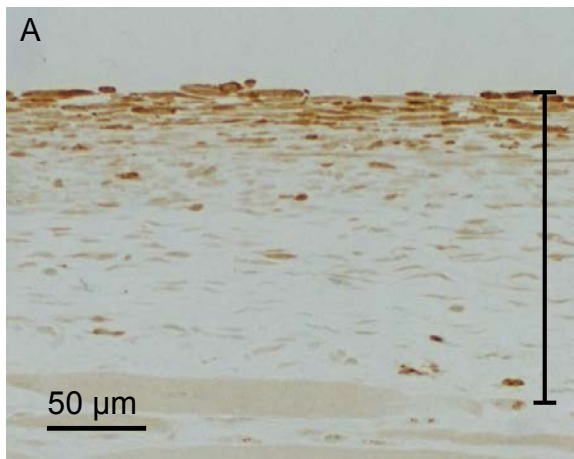


**Fig 3**

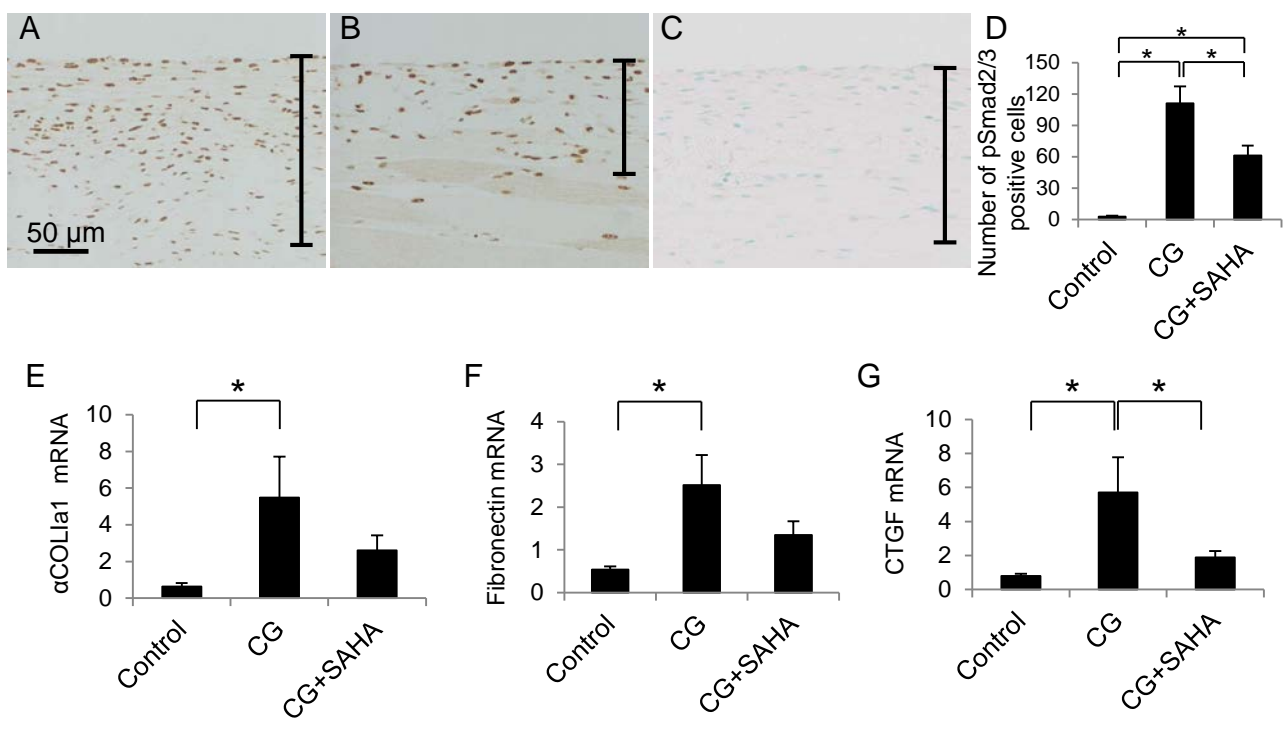


**Fig 4**

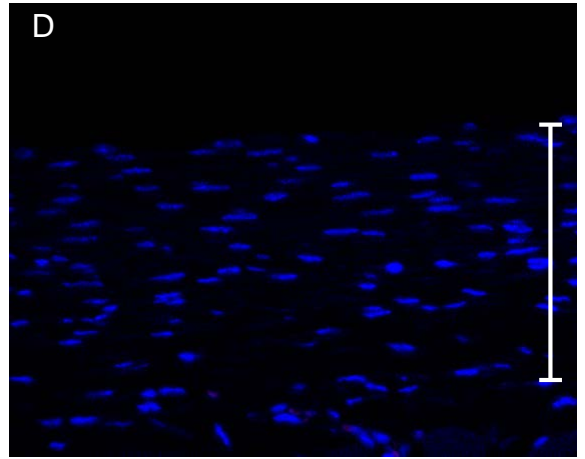
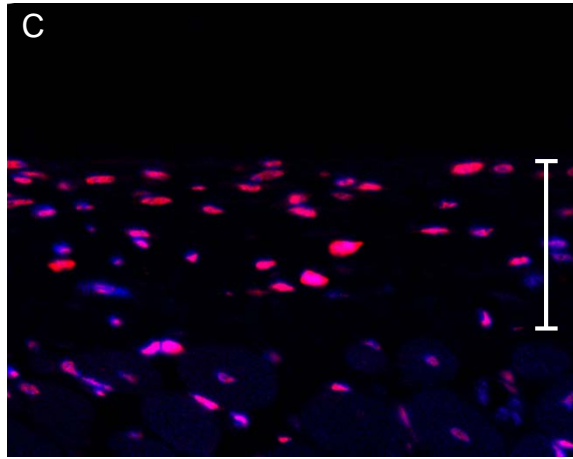
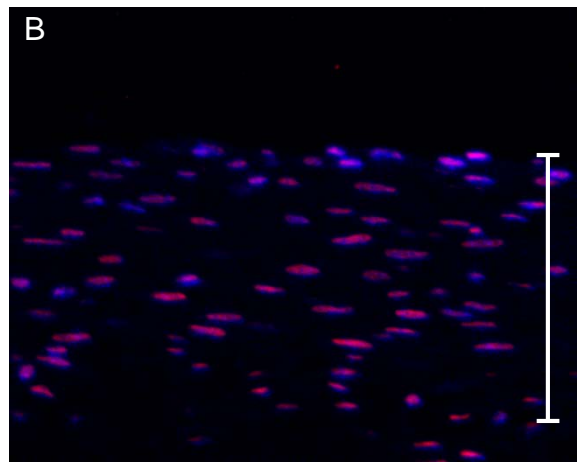
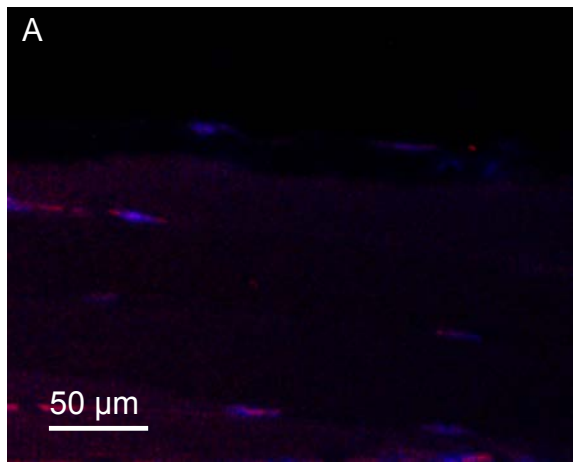
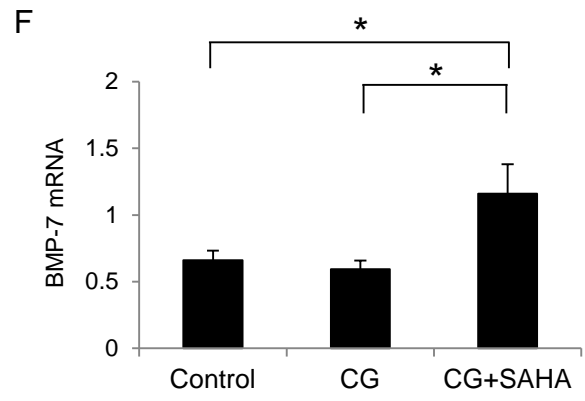
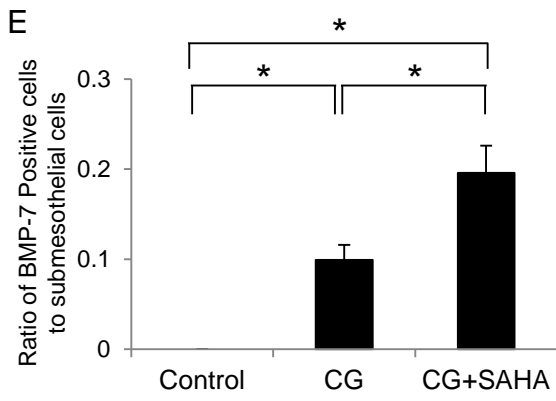
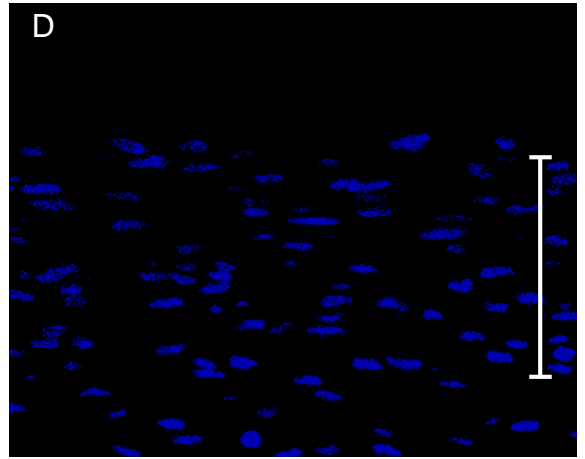
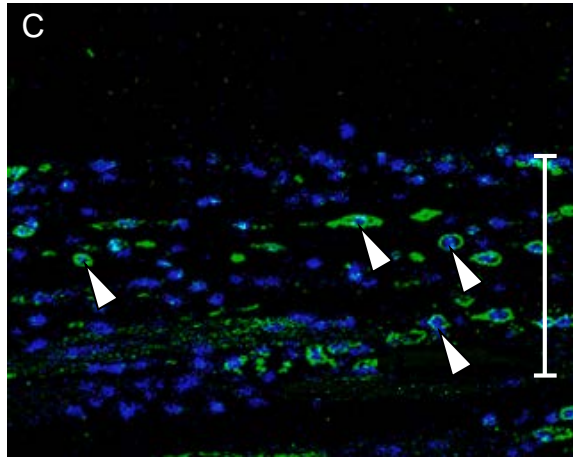
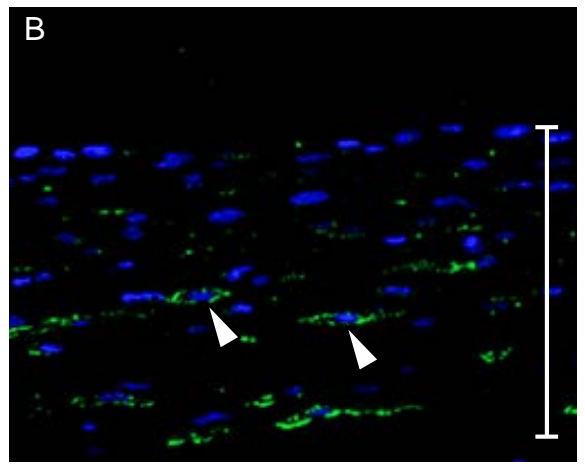
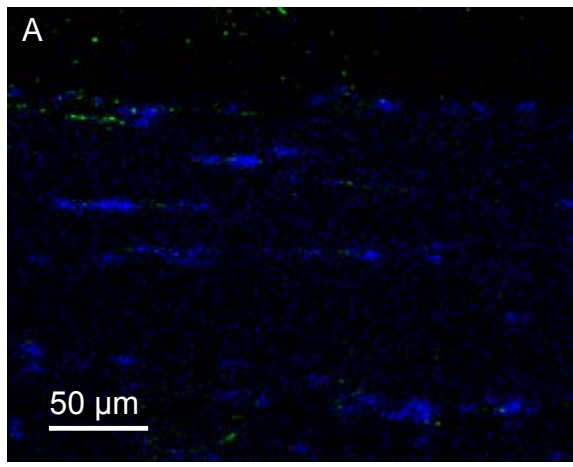
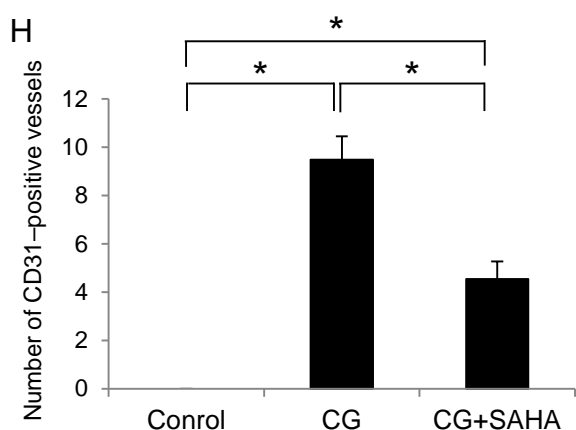
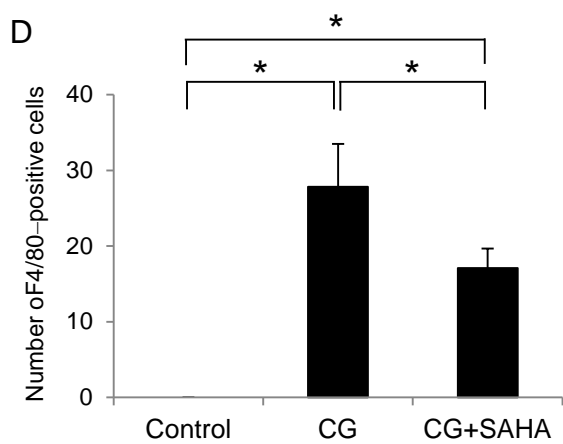
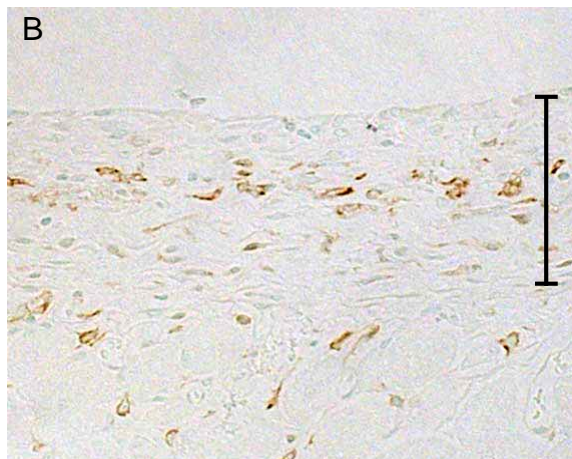
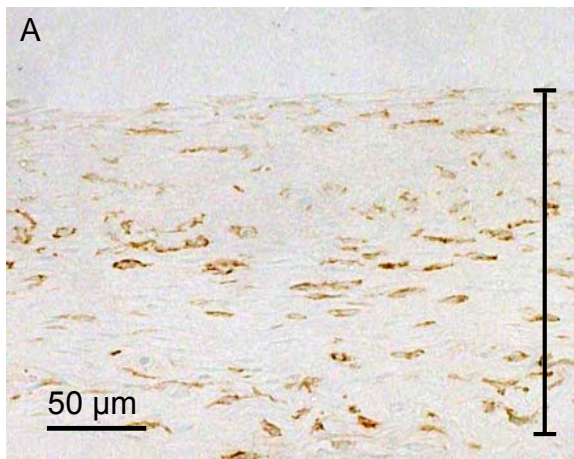


Fig 5



**Fig 6**



**Fig 7**